Washington University School of Medicine

Digital Commons@Becker

10-1-2023

In silico trial of simulation-free hippocampal-avoidance whole brain adaptive radiotherapy

Alex T Price
Washington University School of Medicine in St. Louis

Kylie H Kang
Washington University School of Medicine in St. Louis

Francisco J Reynoso
Washington University School of Medicine in St. Louis

Eric Laugeman
Washington University School of Medicine in St. Louis

Christopher D Abraham
Washington University School of Medicine in St. Louis

See next page for additional authors

Follow this and additional works at: https://digitalcommons.wustl.edu/oa_4

Part of the Medicine and Health Sciences Commons

Please let us know how this document benefits you.

Authors

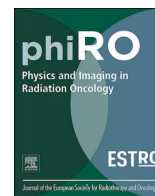Alex T Price, Kylie H Kang, Francisco J Reynoso, Eric Laugeman, Christopher D Abraham, Jiayi Huang, Jessica Hilliard, Nels C Knutson, and Lauren E Henke

Original Research Article

In silico trial of simulation-free hippocampal-avoidance whole brain adaptive radiotherapy

Alex T. Price [1,*], Kylie H. Kang, Francisco J. Reynoso, Eric Laugeman, Christopher D. Abraham, Jiayi Huang, Jessica Hilliard, Nels C. Knutson, Lauren E. Henke [1]

Department of Radiation Oncology, Washington University School of Medicine, 4511 Forest Park Ave, St. Louis, MO 63108, USA

ABSTRACT

Background and Purpose: Hippocampal-avoidance whole brain radiotherapy (HA-WBRT) can be a time-consuming process compared to conventional whole brain techniques, thus potentially limiting widespread utilization. Therefore, we evaluated the *in silico* clinical feasibility, via dose-volume metrics and timing, by leveraging a computed tomography (CT)-based commercial adaptive radiotherapy (ART) platform and workflow in order to create and deliver patient-specific, simulation-free HA-WBRT.
Materials and methods: Ten patients previously treated for central nervous system cancers with cone-beam computed tomography (CBCT) imaging were included in this study. The CBCT was the adaptive image-of-the-day to simulate first fraction on-board imaging. Initial contours defined on the MRI were rigidly matched to the CBCT. Online ART was used to create treatment plans at first fraction. Dose-volume metrics of these simulation-free plans were compared to standard-workflow HA-WBRT plans on each patient CT simulation dataset. Timing data for the adaptive planning sessions were recorded.
Results: For all ten patients, simulation-free HA-WBRT plans were successfully created utilizing the online ART workflow and met all constraints. The median hippocampi $D_{100\%}$ was 7.8 Gy (6.6–8.8 Gy) in the adaptive plan vs 8.1 Gy (7.7–8.4 Gy) in the standard workflow plan. All plans required adaptation at first fraction due to both a failing hippocampal constraint (6/10 adaptive fractions) and sub-optimal target coverage (6/10 adaptive fractions). Median time for the adaptive session was 45.2 min (34.0–53.8 min).
Conclusions: Simulation-free HA-WBRT, with commercially available systems, was clinically feasible via plan-quality metrics and timing, *in silico*.

1. Introduction

Hippocampal-avoidance whole brain radiation therapy (HA-WBRT) limits radiation dose to the hippocampal-region. This technique has been shown to better preserve cognitive function in patients with brain metastases outside of the hippocampal-avoidance region with no difference in intracranial progression-free and overall survival [1–4]. However, HA-WBRT requires potentially longer planning times when compared to conventional WBRT (5–10 business days, compared to as quickly as within 24 h). This is due to the comparative complexity of plan styles used: volumetric modulated arc therapy (VMAT) and intensity modulated radiotherapy (IMRT) for HA-WBRT versus two-dimensional planning used for conventional WBRT. Brain metastases

can grow in as rapidly as one week and are highly morbid, with the median survival time of one month in untreated patients, and thus can lead to urgent clinical scenarios that require foregoing HA-WBRT in order to deliver timely treatment (i.e., WBRT) at the expense of neuro-cognitive preservation [5].

One potential solution to a quicker plan turnaround time is to utilize simulation-free approaches. Simulation-free workflows with conventional linacs and diagnostic imaging have been implemented in simple palliative settings with the use of 3-dimensional (3D) fields [6,7]. However, this approach is limited by the anatomical changes between the diagnostic imaging session and treatment where positional or target changes can be expected. Therefore, the use of adaptation at first fraction to better match the observed "anatomy-of-the-day" as seen on on-

board treatment images can be used to create an original plan [8–10]. To date, the treatment targets in simulation-free approaches are relatively lower in complexity such bony or large lung metastases and have minimal dose-volume objectives to limit planning complexity. However, cone-beam CT (CBCT) adaptation can be clinically implemented in wide-variety of clinical settings with varying levels of complexity [11–15]. Therefore, the use of simulation-free adaptive approaches in complex treatment settings is possible. The use of simulation-free adaptive radiotherapy (ART) in complex treatment scenarios, such as HA-WBRT has not been reported to date.

We have developed an institutional simulation-free HA-WBRT workflow, using a commercially available, CT-based online ART platform. Additionally, we aimed to create a methodology that can be performed with the proposed adaptive system in combination with a commercially available treatment planning system or image registration software, thus making it broadly accessible. Here, we evaluate this novel workflow, *in silico*, for the creation of patient-specific, simulation-free HA-WBRT plans. We hypothesized that simulation-free HA-WBRT would be clinically feasible, *in silico*, by assessing dose-volume metric compliance and timing information.

2. Materials and methods

2.1. Patient selection

Ten patients previously treated for central nervous system (CNS) cancers with adequate diagnostic brain magnetic resonance images (MRI), simulation CT, and daily CBCT imaging and suitable anatomy for this study were identified. All patients in this study were included in an institutional review board protocol (#202009080). Specifically, patients included were selected from those clinically treated for CNS cancers on a TrueBeam Edge linear accelerator (Varian Medical Systems, Palo Alto, CA) at our institution in 2021. This machine was chosen for the *in silico* analysis due to the superior image quality of the on-board CBCT compared to other linear accelerators at our institution, which would best approximate the high-resolution quality of the CBCT on a ring gantry CT-guided linear accelerator, Ethos (Ethos, Varian Medical Systems, Palo Alto, CA) [16,17]. Finally, included patients also had a high-resolution, thin-slice diagnostic brain MRI.

2.2. Pretreatment imaging and contouring workflow

The basis of our simulation-free workflow was use of the diagnostic MRI for patient-specific anatomy. Simulation-free plans (SF-HAWBRT) by definition do not include information from a patient-specific simulation CT. However, the adaptive treatment planning system (TPS) (Ethos Version 1.1) requires that a CT image serves as the primary dataset for plan calculation; a diagnostic brain MRI cannot be used as the primary dataset. Therefore, an alternative method for inserting a CT into the planning process was necessary, to satisfy the primary dataset requirement of the adaptive TPS and to provide electron density information for plan calculation.

An atlas-based registration technique was used as the alternative method to register the patient specific MRI with a library of existing CT images to find the CT image within the library that most closely matches the patient-specific image [18]. The best matched CT, also called atlas-based CT (AB-CT), was then imported into the adaptive TPS with the patient-specific brain MRI registered as the secondary image. The AB-CT was used only for electron density information and did not contribute to any anatomical contour segmentation within the treatment plan. The relevant HA-WBRT structures (brain, brainstem, optic nerves, optic chiasm, eyes, lens, hippocampi) were contoured using the patient-specific MRI registered to the AB-CT. Additionally, ventricles were contoured using the MRI to aid in patient alignment at the machine, since the ventricles are well-visualized on a CBCT image. The contours as drawn based on the MRI were associated with the AB-CT and used for

pre-plan calculation and assessment. Further details of the atlas-based registration method and figures relating to the overall *in silico* simulation-free workflow is presented in the supplementary materials.

2.3. Preplan creation

Each treatment pre-plan used a HA-WBRT simulation-free treatment template (created by our institution) within the adaptive TPS and were not modified on a per-patient basis [19]. A three full-arc plan geometry with isocenter at mid-brain and collimators at 15-, 45-, and 90-degrees was generated in Eclipse (Varian Medical Systems, Palo Alto, CA) and used for the adaptive treatment plan calculation, using the AB-CT electron density information. Because the AB-CT plan was to be deformed to the patient-specific CBCT, thus creating a new primary CT dataset, detailed review of the isodose distribution was not required, as it would change with the on-table CBCT. The objectives used for treatment planning were also extracted from NRG CC001 and presented in Table 1 [4].

2.4. Plan adaptation workflow

At the time of plan adaptation, which was performed to create the final SF-HAWBRT plan, the patient-specific CBCT from the C-arm linac was injected into the emulator system (Varian Medical Systems, Palo Alto, CA). Then, the AB-CT was deformed to the patient-specific CBCT to provide appropriate electron density information for final SF-HAWBRT plan calculation. Instead of deforming the clinical target volume (CTV), the default process in the commercial adaptive system, the CTV contour was rigidly copied from the pre-plan AB-CT (which had contours based on the diagnostic brain MRI anatomy) onto the patient-specific CBCT. This rigid copy process was then repeated for transfer of organ-at-risk (OAR) contours within the CTV onto the patient-specific CBCT while also maintaining their spatial relationship within the brain via a constellation registration. This process meant that when the parent contour (i.e., CTV, which houses within it the critical OARs) was translated or rotated by a certain degree, the offspring contours (i.e., hippocampi, brainstem, ventricles, optic chiasm) would translate or rotate by that same magnitude.

The unedited brain, ventricles, and brainstem contours were used to aid in the translational/rotational alignment of all the above mentioned rigidly copied structures onto the patient-specific CBCT. Therefore, when the brain, ventricle, and brainstem were all well-aligned via this constellation registration method, the chiasm and hippocampi were also expected to be well-aligned to the anatomy initially defined on the patient-specific diagnostic MRI. Finally, the brain, lens, optic chiasm (if visible), optic nerves, and face-avoid structures were re-contoured as needed based on patient anatomy-of-the-day as seen on the patient-specific CBCT. Neither the brainstem, ventricles, nor the hippocampus were adjusted during this step as they maintain their spatial relationship once rigidly copied. The brain was only adjusted at the bone interface where there may have been slight differences in contouring on the MRI when compared to the CBCT. A Planning Target Volume (PTV) was generated, consisting of the hippocampal avoidance region (hippocampi contour + 5 mm circumferential margin) subtracted from the brain contour. Plan optimization then occurred once contours were approved. The adaptive plan was chosen for treatment after re-optimization if the plan met all objectives. Detailed timing information was collected during the *in silico* simulated workflow for each step of the on-table ART process. Successful creation of this adaptive-based SF-HAWBRT plan that met all pre-specified plan constraints and performed in less than one hour was counted as a clinically successful *in silico* treatment.

2.5. Plan quality verification

In order to verify that the plan calculated using the SF-HAWBRT workflow had plan quality metrics comparable to a plan calculated

Table 1

Presentation and comparison of dose-volume metrics for the simulation free, verification, and traditional HAWBRT workflows.

Structure cm^3	Dose-Volume Parameter	Constraint (Variation Acceptable)	SF-HAWBRT Median (Min–Max)	Veri-HAWBRT Median (Min–Max)	Trad-HAWBRT Median (Min–Max)	Difference between SF-HAWBRT& Trad-HAWBRT (sign test, p-value)
	Volume (cm^3)	–	1637.3	–	1636.8	0.75
PTV_3000	D$_{2\%}$(Gy)	≤ 37.5 (37.5 to 40)	33.9 (33.4–35.2)	34.1 (33.3–35.5)	32.5 (32.4–32.9)	0.34
	D$_{98\%}$(Gy)	≥ 25 (22.5 to 25)	28.2 (27.8–28.7)	28.4 (27.8–28.8)	26.2 (24.7–26.6)	0.75
	V30$_{Gy}$(%)	≥ 95 (90 to 95)	95.7 (95.2–96.3)	96.0 (94.9–96.5)	89.3 (88.6–91.1)	0.75
Hippocampi	D$_{100\%}$(Gy)	≤ 9 (9 to 10)	7.8 (6.6–8.8)	7.7 (6.7–9.2)	8.1(7.7–8.4)	0.75
	D$_{0.03cm3}$(Gy)	≤ 16 (16 to 17)	14.0 (12.3–14.8)	14.3 (12.0–16.3)	12.1 (10.1–13.3)	0.75
OpticNerve_L	D$_{0.03cm3}$(Gy)	≤ 30 (30 to 37.5)	28.6 (22.8–29.0)	28.5 (23.4–30.3)	27.6 (25.5–28.5)	1.0
OpticNerve_R	D$_{0.03cm3}$(Gy)	≤ 30 (30 to 37.5)	28.4 (22.4–29.4)	28.9 (21.8–30.6)	27.6 (26.1–28.9)	1.0
OpticChiasm	D$_{0.03cm3}$(Gy)	≤ 30 (30 to 37.5)	29.1 (28.3–29.5)	29.2 (27.7–29.7)	29.0 (28.8–29.3)	0.75

using a simulation CT, the adaptive plan (which used contours based off the diagnostic brain MRI and tweaked for day-of anatomy using the CBCT) was recalculated on the patient-specific simulation CT that had been obtained for the patient's actual CNS treatment. The isocenter (at imaging isocenter) from the SF-HAWBRT plan was then used as the isocenter of the plan on the simulation CT and was placed by registering the two images together. Additionally, the contours from the SF-HAWBRT plan were then transferred onto the simulation CT and not adjusted. This verification calculation is henceforth referred to as the Veri-HAWBRT plan. The dose-volume histograms (DVH) from the adapted SF-HAWBRT plans and the patient-specific Veri-HAWBRT plans were compared using a dose-difference along all DVH points. These two dose calculations were then compared to a HA-WBRT plan optimized

using the patient-specific planning CT and standard clinical planning approaches at our institution [20]. This will be henceforth referred to as the Trad-HAWBRT plan. In this comparison, dose-volume objectives from NRG CC001 were used.

Plan comparisons between the SF-HAWBRT vs. Trad-HAWBRT plans were performed using the sign test. This test was chosen given the non-normal, non-symmetric distribution of data between the pre- and post-value differences. A p-value ≤ 0.05 was considered statistically significant. Statistical tests were performed using IBM SPSS Statistics version 28.0.0.0.
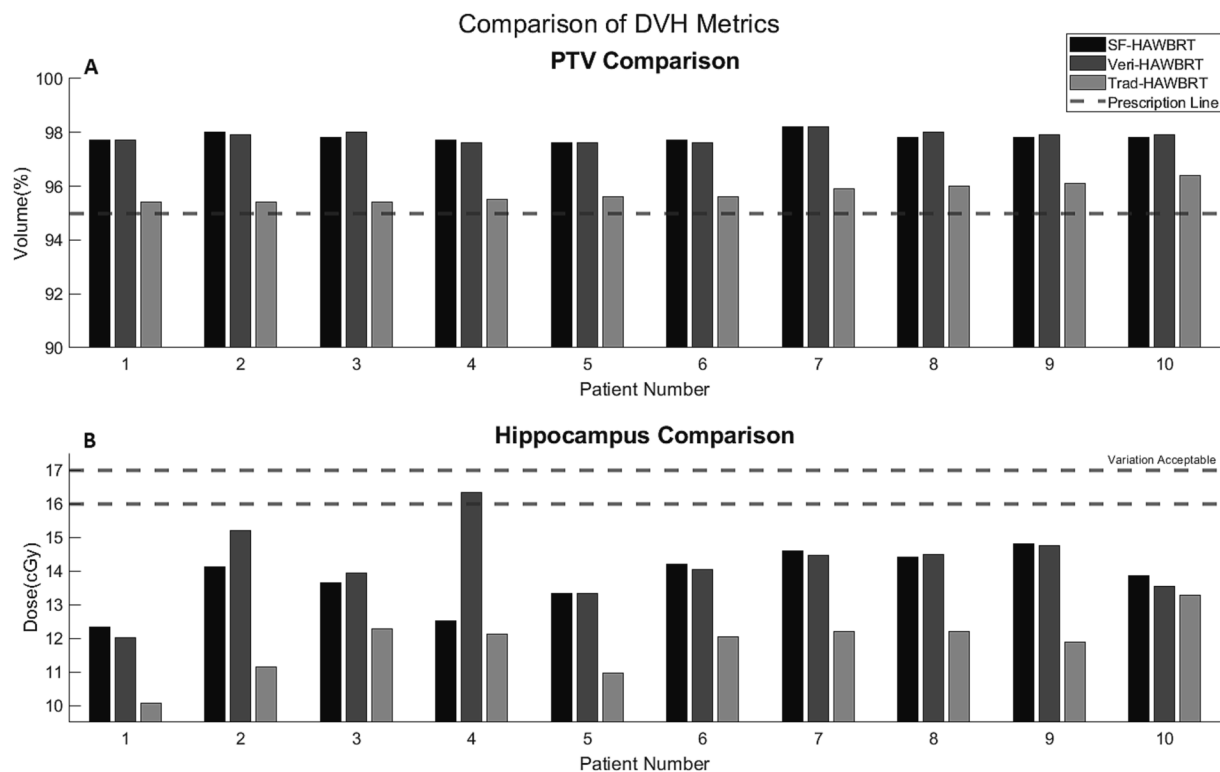

Fig. 1. Patient-specific dose differences for (A) planning target volume (PTV) coverage and (B) hippocampal dose relative to goal prescription coverage and goal hippocampal sparing constraints across simulation-free (SF), verification (Veri) and traditional simulation (Trad) plan types.

3. RESULTS

The SF-HAWBRT workflow created adaptive treatment plans that met all NRG CC001 dose-volume objectives for all ten patients. With regards to coverage, the median PTV V30Gy in the SF-HAWBRT workflow were 95.7% (95.2–96.3%). With regards to hippocampal dose, the SF-HAWBRT plans achieved hippocampal sparing with a median D100% of 7.8 Gy (6.6–8.8 Gy) and D0.03 cm^3 of 14.0 Gy (12.3–14.8 Gy).

Fig. 1 illustrates the numeric differences in target coverage and hippocampal sparing achieved across plan types for each individual patient, relative to the dose-volume constraint objectives. Numerically, the Trad-HAWBRT method resulted in lower PTV coverage, 89.3% (88.6–91.1%), but was not statistically significant via Sign test (p > 0.05). Detailed plan comparison data are presented in Table 1.

When comparing the SF-HAWBRT and Veri-HAWBRT plans, the absolute value of any dose difference for each plan type were less than 1.0 Gy across all DVH points and metrics for 9/10 patients (Fig. 2). In one of the patients, the right hippocampus dose was markedly higher in the verification plan, with a dose difference of 2.6 Gy. The median dose difference in the right/left hippocampus and PTV combined was −0.1 Gy (inter-quartile range: 0.2 Gy) for all three structures.

The median time for the *in silico* on-table adaptation workflow was 45.2 min (34.0–53.8 min). The longest step during this process was contour adjustment for targets and OARs with a median time of 22.6 min (12.6–28.7 min). The median time for influencer contour structures was 4.4 min (2.6–7.8 min), while target propagation and alignment was 4.3 min (3.0–7.6 min), dose calculation was 12.5 min (10.3–14.6 min), and physician plan evaluation was 0.9 min (0.4–1.7 min).

With regards to the impact of first-fraction adaptation for simulation-free plans, adaptation was necessary for dose-volume objective compliance for SF-HAWBRT plans (Table 2). Prior to first-fraction adaption, 6/10 patients' "scheduled" plans failed at least one hippo-campal sparing objective when previewed upon the 1st fraction treatment anatomy/head position. Similarly, 6/10 patients' scheduled plans failed PTV coverage objectives prior to plan adaptation. In aggregate, all 10 patients had at least one dose-volume objective that failed NRG CC001 constraints prior to first-fraction plan adaptation.

4. Discussion

In this study, we demonstrated that a simulation-free HA-WBRT workflow is feasible, *in silico,* and produces plans that are clinically similar to a traditional, simulation-based workflow. This simulation-free workflow leverages a commercially-available, online ART platform in order to allow for creation of pre-plans based on patient-specific diagnostic MRIs and refine them at first fraction using online adaptation to account for differences in head position between diagnostic and on-table imaging. Additionally, this methodology can be executed by clinics who only have access to the proposed adaptive system and a separate TPS to perform image registrations. This workflow could be used clinically to expedite time to delivery of HA-WBRT without compromising plan quality.

For this methodology to be successful, we needed to demonstrate that there were minimal differences between using a deformed AB-CT to the patient-specific CBCT and the patient-specific simulation CT. We were able to show that the hippocampus max doses were always within NRG CC001 tolerance and similar between the AB-CT and patient-specific simulation CT calculations. As for the patient with larger differences in the hippocampus dose, we were not specifically able to isolate the cause of the difference, but we hypothesize that it is due to uncertainties in the deformation of the AB-CT and registration/transfer of contours between the CBCT and simulation CT relative to the adaptive plan coordinate system. For added context, many conventional 3D whole brain treatments often use hand-calculations that assume homogenous water [21]. Additionally, Gamma Knife radiotherapy has also used a homogenous water density assumption during their calculation for many years [22]. The data presented here show similar plan quality and consistency to these established workflows and indicate that this simulation-free HAWBRT workflow is safe and will appropriately deliver palliative doses.

Another potential failure mode of this complex, simulation-free methodology would be the inability to appropriately align the patient using only the patient's contours derived from the diagnostic MRI. While alignment directly to a soft tissue structure such as the hippocampi could prove to be challenging using standard CBCT alignment, we found that inclusion of the brainstem and ventricles as well as the CTV (brain) relative to the skull allowed us to triangulate the position of the hippocampi appropriately. The use of surrogates for alignment is common practice within radiation oncology, including highly conformal, stereotactic, curative-intent strategies, including the daily alignment for brain stereotactic radiosurgery [23–25]. Additionally, we believe that the uncertainties introduced during this process are no greater than the combined uncertainties of traditional HA-WBRT from simulation to
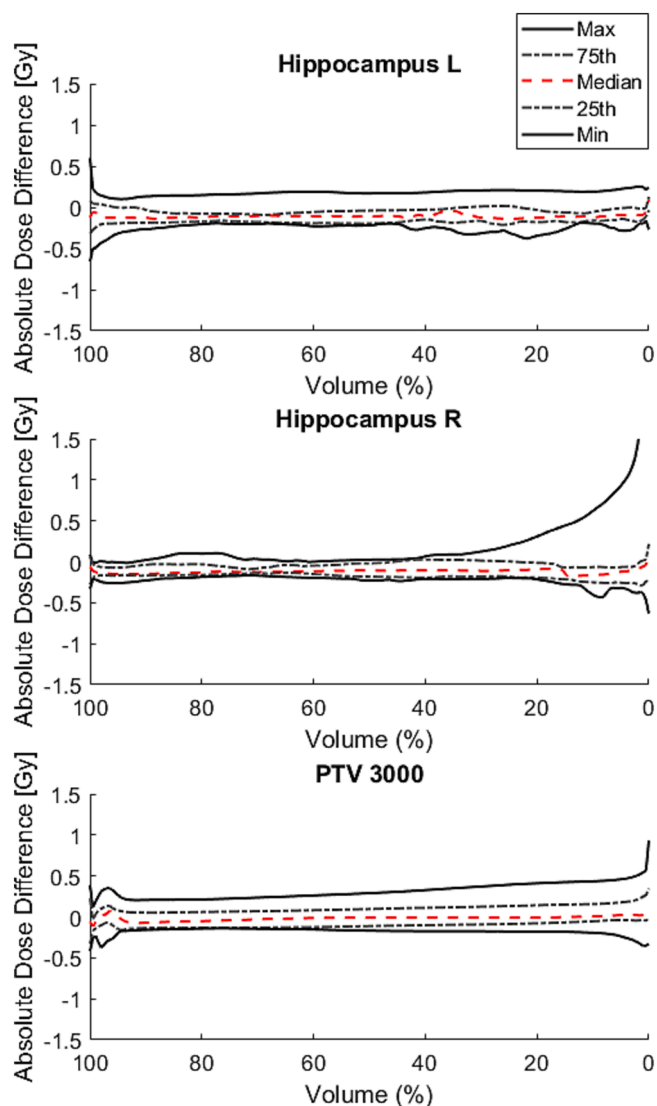

Fig. 2. For comparing the SF-HAWBRT and Veri-HAWBRT plans, the absolute dose difference was calculated at each volumetric point for each patient. The minimum, 25th percentile, median, 75th percentile, and maximum dose differences across all patients were subsequently calculated. These range values of the absolute dose differences (in Gy) are plotted as a function of volume (in %) for our study cohort (*n* = 10). All reported differences were less than 1 Gy except for a single patient's right hippocampus; all objectives met per NRG CC001 constraints.

Table 2
Comparison of dose-volume metrics in the scheduled vs. adapted simulation-free HA-WBRT treatment plans.

Structure	Dose-volume Parameter	Constraint (Variation Acceptable)	Number of constraint violations in initial plan	Initial plan Median (Min–Max)	Number of violations in adapted plan	Adapted plan Median (Min–Max)
PTV_3000	$D_{2\%}$(Gy)	≤ 37.5 (37.5 to 40)	0	34.2 (33.4–35.2)	0	33.9 (33.4–35.2)
	$D_{98\%}$(Gy)	≥ 25 (22.5 to 25)	3	24.2 (19.4–27.3)	0	28.2 (27.8–28.7)
	$V30_{Gy}$(%)	≥ 95 (90 to 95)	6	89.6 (84.8–93.9)	0	95.7 (95.2–96.3)
Hippocampi	$D_{100\%}$(Gy)	≤ 9 (9 to 10)	0	7.8 (7.4–9.7)	0	7.8 (6.6–8.8)
	D_{max}(Gy)	≤ 16 (16 to 17)	6	18.6 (14.1–29.9)	0	14.0 (12.3–14.8)
OpticNerve_L	D_{max}(Gy)	≤ 30 (30 to 37.5)	0	30.4 (28.3–32.9)	0	28.6 (22.8–29.0)
OpticNerve_R	D_{max}(Gy)	≤ 30 (30 to 37.5)	0	30.3 (25.0–32.2)	0	28.4 (22.4–29.4)
OpticChiasm	D_{max}(Gy)	≤ 30 (30 to 37.5)	0	30.4 (28.8–34.3)	0	29.1 (28.3–29.5)

treatment. This includes MRI to CT image registration, which carries an uncertainty of up to 1.5 mm [26,27] and the registration of the CBCT to simulation CT, which carries an additional 1.5 mm in uncertainty [27]. Also, HA-WBRT traditionally incorporates a hippocampal avoidance region, which is a 5 mm expansion upon the hippocampi themselves to allow for some margin for daily uncertainties in these palliative intent patients, as well as for dose fall-off [28,29]. Therefore, we believe that the uncertainties accepted in a traditional planning process relating to localization are similar to the uncertainties produced in our method, and thus our method is appropriate for this palliative-intent treatment paradigm.

Timing was an important part of the simulation-free HA-WBRT process, as patients with brain metastases are often less medically stable and on-table efficiency is paramount. For context, at our institution, all CT simulations are scheduled within one-hour time blocks. We demonstrated here that the patient would be on the treatment table for the CBCT, contouring, plan calculation, and quality assurance for less than the duration of a traditional CT simulation timeslot at our institution. Additionally, the plan adaptation in the clinical application of hippocampal-avoidance whole brain radiotherapy is not anticipated to require any additional time compared to previously reported CT-based adaptive radiotherapy, which is on the order of 15–30 min [9,12], or a separate 3D WBRT simulation-free approach, which was approximately 25–45 min [30]. Additionally, as on-table adaptation tools continue to mature in future releases of commercial adaptive systems, such as increased and improved auto-contouring tools along with direct CBCT plan calculation, we expect that on-table time will continue to decrease, thus becoming more efficient.

The simulation-free methodology is successful and feasible in the setting of HA-WBRT in large part due to the standardized approach of HA-WBRT and similar anatomy between patients. This combination of factors allows for template-based planning [20,31]. The adaptive TPS is designed to use template-based planning for maximizing efficiency [32]. In this simulation-free setting, this enables rapid generation of the diagnostic imaging-based pre-plan, which is then refined on-table. When thinking about extending this methodology outside the setting of HA-WBRT, any anatomical site that has consistent anatomy or extremely regimented approaches could be similarly approached [9].

Despite this methodology's overall success, there is still more to gain in improving the process's efficiency. For example, a synthetic CT generated from an MRI would have eliminated the need for atlas-based registration. However, not all MRIs come from our institution, where we can control the MRI used, nor does every facility have access to advanced and possibly costly software algorithms to perform synthetic CT generation [33,34]. As for the use of a patient-specific diagnostic CT

for the primary dataset, not all patients who present with brain metastases who are receiving HA-WBRT have a diagnostic CT that encompasses the whole brain or the diagnostic CT is not within the hospital PACs system. Additionally, the use of an outside hospital diagnostic CT may have unverified Hounsfield unit values [35]. Therefore, our methodology aims to be broadly accessible and to enable more facilities to implement this process. However, we do endorse the use of methods that may increase efficiency of this approach. Despite future improvements, our proposed method still demonstrates that simulation-free HA-WBRT is possible and has not been reported to date.

To conclude, we found that simulation-free HA-WBRT was clinically safe, *in silico*, by applying first fraction on-table adaptation in order to refine a diagnostic imaging-based pre-plan to match the anatomy of the treatment position. Use of a simulation-free process like that delineated here may reduce time-to-treatment for HA-WBRT, allowing patients urgently requiring treatment for brain metastases to benefit from both timely radiotherapy delivery as well as maximal cognitive sparing. A phase I prospective clinical trial has finished accruing at our institution and will allow us to evaluate this approach *in vivo*.

CRediT authorship contribution statement

Alex T. Price: Conceptualization, Methodology, Investigation, Visualization. **Kylie H. Kang:** Formal analysis, Investigation. **Francisco J. Reynoso:** Methodology, Resources. **Eric Laugeman:** Methodology, Investigation, Project administration. **Christopher D. Abraham:** Methodology. **Jiayi Huang:** Data curation, Methodology. **Jessica Hilliard:** Investigation, Data curation. **Nels C. Knutson:** Methodology. **Lauren E. Henke:** Conceptualization, Funding acquisition, Supervision.

Declaration of Competing Interest

Honoraria from Varian Medical Systems, Inc. is reported by Francisco Reynoso and Lauren Henke. Honoraria from ViewRay is reported by Lauren Henke and Alex Price. Lauren Henke reports consulting fees from Varian Medical Systems and Radialogica. Lauren Henke is on the CNS and medical advisory board for ViewRay.

Appendix A. Supplementary data

Supplementary data to this article can be found online at https://doi.

org/10.1016/j.phro.2023.100491.

References

[1] Gondi V, Tomé WA, Mehta MP. Why avoid the hippocampus? A comprehensive review Radiother Oncol 2010;97:370–6. https://doi.org/10.1016/j.radonc.2010.09.013.

[2] Brown PD, Pugh S, Laack NN, Wefel JS, Khuntia D, Meyers C, et al. Memantine for the prevention of cognitive dysfunction in patients receiving whole-brain radiotherapy: a randomized, double-blind, placebo-controlled trial. Neuro Oncol 2013;15:1429–37. https://doi.org/10.1093/neuonc/not114.

[3] Gondi V, Pugh SL, Tome WA, Caine C, Corn B, Kanner A, et al. Preservation of memory with conformal avoidance of the hippocampal neural stem-cell compartment during whole-brain radiotherapy for brain metastases (RTOG 0933): a phase II multi-institutional trial. J Clin Oncol 2014;32:3810–6. https://doi.org/10.1200/JCO.2014.57.2909.

[4] Brown PD, Gondi V, Pugh S, Tome WA, Wefel JS, Armstrong TS, et al. Hippocampal Avoidance During Whole-Brain Radiotherapy Plus Memantine for Patients With Brain Metastases: Phase III Trial NRG Oncology CC001. J Clin Oncol 2020;38: 1019–29. https://doi.org/10.1200/JCO.19.02767.

[5] Zimm S, Wampler GL, Stablein D, Hazra T, Young HF. Intracerebral metastases in solid-tumor patients: natural history and results of treatment. Cancer 1981;48: 384–94. https://doi.org/10.1002/1097-0142(19810715)48:2<384::aid-cncr2820480227>3.0.co;2-8.

[6] Schuler T, Back M, Hruby G, Carroll S, Jayamanne D, Kneebone A, et al. Introducing Computed Tomography Simulation-Free and Electronic Patient-Reported Outcomes-Monitored Palliative Radiation Therapy into Routine Care: Clinical Outcomes and Implementation Experience. Adv Radiat Oncol 2021;6: 100632. https://doi.org/10.1016/j.adro.2020.100632.

[7] Schiff JP, Zhao T, Huang Y, Sun B, Hugo GD, Spraker MB, et al. Simulation-Free Radiation Therapy: An Emerging Form of Treatment Planning to Expedite Plan Generation for Patients Receiving Palliative Radiation Therapy. Adv Radiat Oncol 2023;8:101091. https://doi.org/10.1016/j.adro.2022.101091.

[8] Schiff JP, Maraghechi B, Chin R-I, Price A, Laugeman E, Rudra S, et al. A pilot study of same-day MRI-only simulation and treatment with MR-guided adaptive palliative radiotherapy (MAP-RT). Clin Transl Radiat Oncol 2023;39. 10.1016/j.ctro.2022.100561.

[9] Nelissen KJ, Versteijne E, Senan S, Rijksen B, Admiraal M, Visser J, et al. Same-day adaptive palliative radiotherapy without prior CT simulation: Early outcomes in the FAST-METS study. Radiother Oncol 2023;182:109538. https://doi.org/10.1016/j.radonc.2023.109538.

[10] Oldenburger E, De Roover R, Poels K, Depuydt T, Isebaert S, Haustermans K. "Scan-(pre)Plan-Treat" Workflow for Bone Metastases Using the Ethos Therapy System: A Single-Center. In Silico Experience Adv Radiat Oncol 2023;8:101258. https://doi.org/10.1016/j.adro.2023.101258.

[11] Zwart LGM, Ong F, Ten Asbroek LA, van Dieren EB, Koch SA, Bhawanie A, et al. Cone-beam computed tomography-guided online adaptive radiotherapy is feasible for prostate cancer patients. Phys Imaging Radiat Oncol 2022;22:98–103. https://doi.org/10.1016/j.phro.2022.04.009.

[12] Sibolt P, Andersson LM, Calmels L, Sjöström D, Bjelkengren U, Geertsen P, et al. Clinical implementation of artificial intelligence-driven cone-beam computed tomography-guided online adaptive radiotherapy in the pelvic region. Phys Imaging Radiat Oncol 2021;17:1–7. https://doi.org/10.1016/j.phro.2020.12.004.

[13] Branco D, Mayadev J, Moore K, Ray X. Dosimetric and feasibility evaluation of a CBCT-based daily adaptive radiotherapy protocol for locally advanced cervical cancer. J Appl Clin Med Phys 2023;24:e13783.

[14] Schiff JP, Price AT, Stowe HB, Laugeman E, Chin R-I, Hatscher C, et al. Simulated computed tomography-guided stereotactic adaptive radiotherapy (CT-STAR) for the treatment of locally advanced pancreatic cancer. Radiother Oncol 2022;175: 144–51. https://doi.org/10.1016/j.radonc.2022.08.026.

[15] Mao W, Riess J, Kim J, Vance S, Chetty IJ, Movsas B, et al. Evaluation of Auto-Contouring and Dose Distributions for Online Adaptive Radiation Therapy of Patients With Locally Advanced Lung Cancers. Pract Radiat Oncol 2022;12: e329–38. https://doi.org/10.1016/j.prro.2021.12.017.

[16] Lassot-Buys M, Verstraet R, Dabli D, Moliner G, Greffier J. Task-Based Image Quality Assessment Comparing Classical and Iterative Cone Beam CT Images on Halcyon®. Diagnostics (Basel) 2023;13. 10.3390/diagnostics13030448.

[17] Henke LE, Fischer-Valuck BW, Rudra S, Wan L, Samson PS, Srivastava A, et al. Prospective imaging comparison of anatomic delineation with rapid kV cone beam CT on a novel ring gantry radiotherapy device. Radiother Oncol 2023;178:109428. https://doi.org/10.1016/j.radonc.2022.11.017.

[18] Martin S, Daanen V, Troccaz J. Atlas-based prostate segmentation using an hybrid registration. Int J Comput Assist Radiol Surg 2008;3:485–92. https://doi.org/10.1007/s11548-008-0247-0.

[19] Ethos Adaptive Planning Templates. Department of Radiation Oncology 2022. https://radonc.wustl.edu/ethos-adaptive-planning-templates/ (accessed March 9, 2023).

[20] Schmidt MC, Abraham CD, Huang J, Robinson CG, Hugo G, Knutson NC, et al. Clinical application of a template-guided automated planning routine. J Appl Clin Med Phys 2022:e13837. 10.1002/acm2.13837.

[21] Stern RL, Heaton R, Fraser MW, Goddu SM, Kirby TH, Lam KL, et al. Verification of monitor unit calculations for non-IMRT clinical radiotherapy: report of AAPM Task Group 114. Med Phys 2011;38:504–30. https://doi.org/10.1118/1.3521473.

[22] Prusator MT, Zhao T, Kavanaugh JA, Santanam L, Dise J, Goddu SM, et al. Evaluation of a new secondary dose calculation software for Gamma Knife radiosurgery. J Appl Clin Med Phys 2020;21:95–102. https://doi.org/10.1002/acm2.12794.

[23] Chang SD, Main W, Martin DP, Gibbs IC, Heilbrun MP. An analysis of the accuracy of the CyberKnife: a robotic frameless stereotactic radiosurgical system. Neurosurgery 2003;52:140–6; discussion 146-7. 10.1097/00006123-200301000-00018.

[24] Chung H-T, Kim JH, Kim JW, Paek SH, Kim DG, Chun KJ, et al. Assessment of image co-registration accuracy for frameless gamma knife surgery. PLoS One 2018; 13:e0193809.

[25] Court LE, Dong L, Taylor N, Ballo M, Kitamura K, Lee AK, et al. Evaluation of a contour-alignment technique for CT-guided prostate radiotherapy: an intra- and interobserver study. Int J Radiat Oncol Biol Phys 2004;59:412–8. https://doi.org/10.1016/j.ijrobp.2003.10.023.

[26] Pappas EP, Seimenis I, Kouris P, Theocharis S, Lampropoulos KI, Kollias G, et al. Target localization accuracy in frame-based stereotactic radiosurgery: Comparison between MR-only and MR/CT co-registration approaches. J Appl Clin Med Phys 2022;23:e13580.

[27] Masitho S, Putz F, Mengling V, Reißig L, Voigt R, Bäuerle T, et al. Accuracy of MRI-CT registration in brain stereotactic radiotherapy: Impact of MRI acquisition setup and registration method. Zeitschrift für Medizinische Physik 2022;32:477–87. https://doi.org/10.1016/j.zemedi.2022.04.004.

[28] Gondi V, Tolakanahalli R, Mehta MP, Tewatia D, Rowley H, Kuo JS, et al. Hippocampal-sparing whole-brain radiotherapy: a "how-to" technique using helical tomotherapy and linear accelerator-based intensity-modulated radiotherapy. Int J Radiat Oncol Biol Phys 2010;78:1244–52. https://doi.org/10.1016/j.ijrobp.2010.01.039.

[29] Park JW, Yea JW, Park J, Oh SA. Setup uncertainties and appropriate setup margins in the head-tilted supine position of whole-brain radiotherapy (WBRT). PLoS One 2022;17:e0271077.

[30] Le AH, Stojadinovic S, Timmerman R, Choy H, Duncan RL, Jiang SB, et al. Real-Time Whole-Brain Radiation Therapy: A Single-Institution Experience. Int J Radiat Oncol Biol Phys 2018;100:1280–8. https://doi.org/10.1016/j.ijrobp.2017.12.282.

[31] Wang S, Zheng D, Zhang C, Ma R, Bennion NR, Lei Y, et al. Automatic planning on hippocampal avoidance whole-brain radiotherapy. Med Dosim 2017;42:63–8. https://doi.org/10.1016/j.meddos.2016.12.002.

[32] Calmels L, Sibolt P, Åström LM, Serup-Hansen E, Lindberg H, Fromm A-L, et al. Evaluation of an automated template-based treatment planning system for radiotherapy of anal, rectal and prostate cancer. Tech Innov Patient Support Radiat Oncol 2022;22:30–6. https://doi.org/10.1016/j.tipsro.2022.04.001.

[33] Lerner M, Medin J, Jamtheim Gustafsson C, Alkner S, Siversson C, Olsson LE. Clinical validation of a commercially available deep learning software for synthetic CT generation for brain. Radiation Oncology 2021;16:66. https://doi.org/10.1186/s13014-021-01794-6.

[34] Kazemifar S, McGuire S, Timmerman R, Wardak Z, Nguyen D, Park Y, et al. MRI-only brain radiotherapy: Assessing the dosimetric accuracy of synthetic CT images generated using a deep learning approach. Radiother Oncol 2019;136:56–63. https://doi.org/10.1016/j.radonc.2019.03.026.

[35] Wong S, Roderick S, Kejda A, Atyeo J, Grimberg K, Porter B, et al. Diagnostic Computed Tomography Enabled Planning for Palliative Radiation Therapy: Removing the Need for a Planning Computed Tomography Scan. Pract Radiat Oncol 2021;11:e146–53. https://doi.org/10.1016/j.prro.2020.10.010.